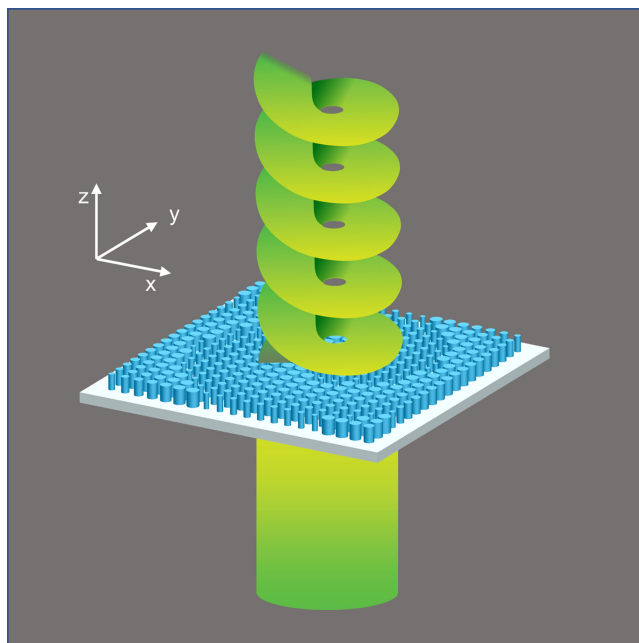


Generation of Optical Vortices With Polarization-Insensitive Metasurfaces



Volume 12, Number 4, August 2020

Z. Shen
R. Li
Y. Z. Xue
Z. Y. Qiu
Z. Y. Xiang
J. Y. Zhou
B. F. Zhang



DOI: 10.1109/JPHOT.2020.3014918

Generation of Optical Vortices With Polarization-Insensitive Metasurfaces

Z. Shen , R. Li, Y. Z. Xue, Z. Y. Qiu, Z. Y. Xiang, J. Y. Zhou,
and B. F. Zhang 

School of Electronic and Optical Engineering, Nanjing University of Science and
Technology, Nanjing 210094, China

DOI:10.1109/JPHOT.2020.3014918

This work is licensed under a Creative Commons Attribution 4.0 License. For more information, see
<https://creativecommons.org/licenses/by/4.0/>

Manuscript received June 22, 2020; revised July 29, 2020; accepted August 4, 2020. Date of publication August 7, 2020; date of current version August 17, 2020. This work was supported in part by the National Natural Science Foundation of China (NSFC) under Grants 61805119 and 61604073, in part by Natural Science Foundation of Jiangsu Province under Grants BK20180469 and BK20160839, and in part by the Fundamental Research Funds for the Central Universities under Grant 30919011275. Corresponding author: Z. shen (e-mail: shenzhe@njjust.edu.cn).

Abstract: Traditionally, optical vortices (OVs) were generated with diffractive optical elements (DOEs) such as spiral phase plate (SPP), fork grating, spatial light modulator (SLM), and liquid crystal display (LCD). Here, a method was proposed for generating OVs by employing all-dielectric polarization-insensitive metasurfaces with cylinder arrays, which have high transmission efficiency. The polarization insensitivity of the metasurfaces was illustrated with the incidence of two pairs of orthogonal polarization, both the phase and transmission efficiency were consistent for the cylinder unit cell, and similar OVs were generated with the cylinder array. The topological charges of the generated OVs can be adjusted through the design of the metasurfaces. OVs with additional characteristics as vector beams, focused beams and Bessel beams were further generated. This work has potential applications in beam shaping, optical tweezers, and optical communication.

Index Terms: Optical vortex, metasurfaces, non-diffraction beam.

1. Introduction

Optical vortex (OV) is a light field with a helical wavefront possessing orbital angular momentum (OAM) [1]. The helical phase distribution of OV is determined by its phase factor $\exp(i\ell\theta)$ [2], where ℓ and θ are topological charge and azimuthal angle, respectively. Because of phase singularity, the phase value at the centre is uncertain, the central intensity of the OV tends to be zero. The applications of OV mainly rely on two distinct characteristics, the OAM related the spiral phase and the central darkness. OAM is associated with the topological charge ℓ , which has unlimited number of eigenmodes (1, 2, 3...), thus offers additional freedom besides wavelength, amplitude and polarization, provides much more information capacity, and finds optical communication applications in both classical and quantum optics [3], [4]. The central darkness of the intensity distribution of OV has been proved to be more suitable for trapping non-transparent or low-refractive-index objects [5], [6]. As a result, the generation, modulation, and application of OV have been widely concerned.

Several diffractive optical elements (DOEs) have been used to generate OVs, for instance, spiral phase plate (SPP) [7], fork grating [8], spatial light modulator (SLM) [9], and liquid crystal display (LCD) [10]. However, these OV generators suffer from a lot of disadvantages, such as bulky size, low efficiency, and narrow working band. In recent years, the use of metasurfaces, a kind of efficient

and compact 2D metamaterials, has been a promising solution to the above-mentioned problems [11], [12]. Metasurface generally consist of a set of subwavelength structure arrays distributed on a planar surface, which can be designed to manipulate the phase, amplitude, polarization and angular momentum of the incident light in a flexible way [13], [14]. Metasurfaces have enriched many frontier fields including beam shaping [12], [15], [16], optical tweezers [17], and optical communication [18], [19]. In 2011, Yu *et al.* arranged the V-shaped antennas in metasurfaces to generate OV [13], opening a new prelude to the development of generating OVs. Generally, there are two typical ways to make $0 \sim 2\pi$ phase change for designing an OV generator through metasurfaces: (i) varying TE and TM resonance parameters [18]; (ii) rotating the orientation of the dipoles [20].

However, these two methods both require the incident light to be in specific polarization states, and the metadevices that have been realized only provide functionality for several defined circular or linear polarized incident light. On the other hand, OVs with different polarization states have attracted widespread attention. Linearly polarized OV has been used to excite surface plasmons for near-field manipulation purposes [21], [22]. Circular polarized OV has been used to prove that light transforms its partial spin angular momentum (SAM) to OAM in a highly focused process [23]. Radially polarized OV has been used to generate plasmonic vortex (PV) for manipulating particles [24], [25]. Azimuthally polarized vortex beam has been used to obtain sub-diffraction-limited focusing [26]. Recently, polarization-insensitive metasurfaces have been proposed and used to make multiwavelength lenses [27], beam splitters [28], broadband metalenses [29], and terahertz devices [30]. Based on varying effective index of each metasurface unit cell [31], the polarization-insensitive metasurfaces have been demonstrated to effectively control wavefront of light [32]–[35]. Therefore, this could provide a way to obtain OVs independently with polarization.

In this work, we designed polarization-insensitive metasurfaces with cylinder arrays to generate OVs, which are transformed from plane waves or Gaussian beams. We first calculated the cylinder radii related phase changes by FDTD method and index waveguide theory for the metasurfaces design. Then the polarization insensitivity of the metasurfaces was examined with the incidence of two pairs of orthogonally polarized beams. Under these conditions, we made the comparisons of the response by the cylinder unit cell with varying radius, and the OV generation by the cylinder array structures. Normal OVs, vector OVs, focused OVs, and Bessel OVs were further obtained on account of potential applications in beam shaping, optical tweezers, and optical communication.

2. Method and Theory

In our design, we used an all-dielectric metasurface consisting of a cylinder array on a glass substrate, as shown in Fig. 1(a). The incident light normally illuminates from the beneath of the substrate, passing through the cylinder array and form an OV. The unit cell shown in Fig. 1 (b) is fabricated with a TiO_2 cylinder and a SiO_2 substrate. The refractive indices of TiO_2 and SiO_2 at working wavelength (532 nm) are 2.43 and 1.46, respectively. The wavelength of 532 nm was used in all simulations throughout this paper. The reason for choosing TiO_2 is that it has a large refractive index and negligible loss in the entire visible region, since the imaginary part in the complex refractive index of TiO_2 is small enough to be ignored in the visible wavelengths. We set the lattice period of the cylinder unit array $p = 250$ nm and the height of the cylinder unit $h = 600$ nm. These two geometric parameters are determined with the constraints described in [36]. On the one hand, the lattice constant should be less than the wavelength in the substrate ($\lambda/n_{\text{SiO}_2} = 364$ nm), according to the Nyquist sampling theorem. On the other hand, it should be greater than $\lambda/2n_{\text{TiO}_2} = 182$ nm, according to the diffraction condition. Under this condition, there exists only zeroth-order diffraction for normal incidence, but it appears there is only feeble first-order diffraction for the oblique incidence case [37], [38]. The maximum exiting phase is given by $\varphi_{\text{max}} = 2\pi(n - 1)d/\lambda$, where d is the thickness of a homogeneous film. The height 600 nm greater than the working wavelength was used to achieve a full $0 \sim 2\pi$ phase coverage. Fig. 1(c) shows a side view of the normalized magnetic energy density of two neighboring nanopillars with radii of 80 nm. It can be seen that light is mainly confined inside the nanostructures due to the waveguiding effect [39] and the coupling between them can be ignored. Fig. 1(d) shows the

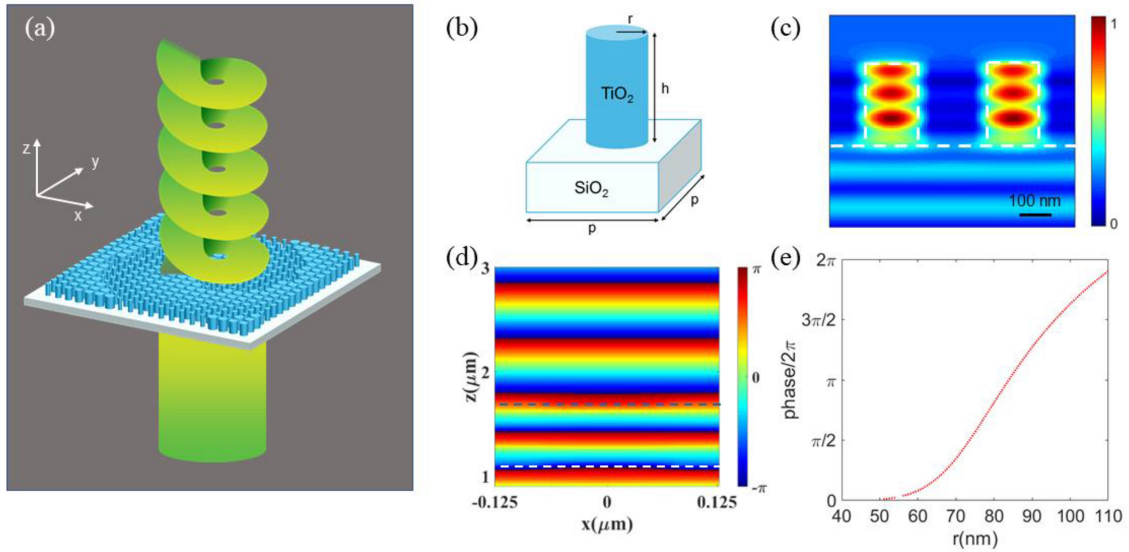


Fig. 1. (a) The schematic of an OV generation through a metasurface. (b) A metasurface unit cell consists of a SiO₂ substrate and a TiO₂ cylinder. With the incidence of *x*-polarized plane wave from bottom, (c) shows a side view of the normalized magnetic energy density for two nanopillars with radii of 80 nm. The white dotted lines indicate the boundaries of the structures. And (d) shows the phase change by a nanopillar with radius of 80 nm. The white dotted line indicates the interface between the TiO₂ cylinder and SiO₂ substrate. The blue dotted line indicates the top surface of the TiO₂ cylinder. (e) The radius dependent theoretical phase curve when $p = 250$ nm.

process of phase change during propagation when the radius of the nanopillar is 80 nm under plane wave illumination. We calculated the relationship between the phase changes of the unit cells and the radii of the cylinders according to the index waveguide theory, as shown in Fig. 1(e). While the radius varies, it can maintain a 2π phase coverage. Then, the required phase profile of the metasurface can be realized by mapping the radii of the cylinders.

To imitate the optical elements involved in the conventional refractive system, we can transfer their phase profiles to the metasurfaces. Eqs. (1), (2) and (3) show the phase profiles of SPP, lens and axicon lens, respectively, which can be used to generate an OV, a focusing beam and a Bessel beam, respectively. Note that beside axicon lens [40], conical diffraction [41], *etc.* can be also used to generate a Bessel beam. “ \pm ” in Eqs. (2) and (3) indicate the divergence and convergence, respectively. Eq. (4) shows the superposition of SPP phase profile and convex lens profile for generating a focused OV. Eq. (5) shows the superposition of SPP phase profile and converging axicon lens profile for generating a Bessel OV.

$$\varphi_{spp} = l \cdot \arctan(y/x) \quad (1)$$

$$\varphi_{lens} = \pm \frac{2\pi}{\lambda} \left(\sqrt{f^2 + x^2 + y^2} - f \right) \quad (2)$$

$$\varphi_{axicon} = \pm \frac{2\pi}{\lambda} \left(\sqrt{x^2 + y^2} \sin \beta \right) \quad (3)$$

$$\varphi_{spp+lens} = l \cdot \arctan(y/x) - \frac{2\pi}{\lambda} \left(\sqrt{f^2 + x^2 + y^2} - f \right) \quad (4)$$

$$\varphi_{spp+axicon} = l \cdot \arctan(y/x) - \frac{2\pi}{\lambda} \left(\sqrt{x^2 + y^2} \sin \beta \right) \quad (5)$$

where λ is the design wavelength, x and y are the coordinates of each cylinder, f is the focal length, β is the base angle of axicon. According to the axicon non-diffraction theory, the maximum

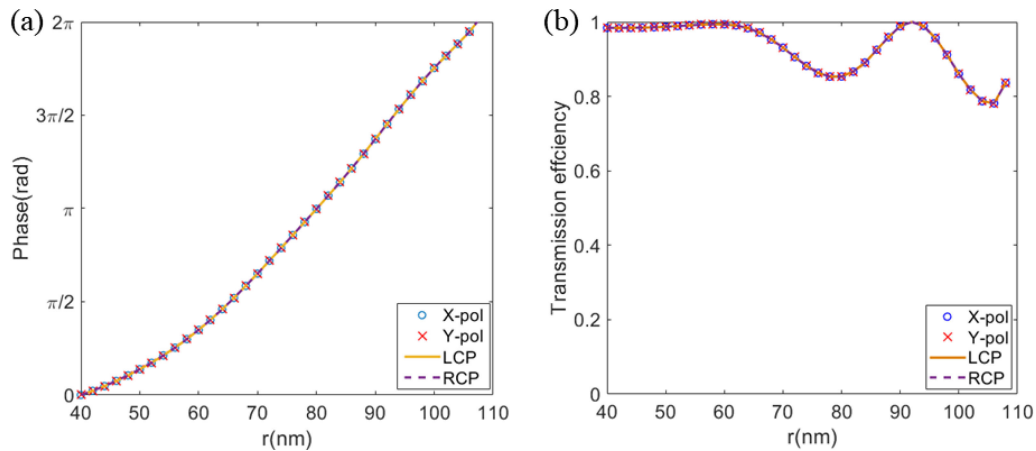


Fig. 2. (a) The relationships between phase changes and radii of the unit cells, and (b) the relationships between transmission efficiency and radii of the unit cells, with the incidence of x -polarized, y -polarized, left-handed circularly polarized and right-handed circularly polarized beams, respectively.

non-diffraction distance of the transmitted beam is proportional to the radius of the surface of axicon and inversely proportional to β [42]. Combining the phase distribution with the relationship between phase and radius, we can obtain exact radius of each cylinder located on the two-dimensional substrate for the design of metasurface.

3. Results and Discussions

3.1 The Polarization Insensitivity of the Metasurfaces

For high-contrast dielectric metasurfaces, the scattering of the cylinders is a local effect and the coupling among them is weak. Thus, the individual response of each unit cell makes sense for the whole metasurface. Owing to the symmetrical geometry of the cylinders, the coefficients (phase and transmission efficiency) should be polarization-independent. To verify the polarization insensitivity of the metasurface unit cells, we calculated the phase changes of the unit cells through FDTD simulations using a commercial software Lumerical (FDTD solutions). Periodic boundary conditions are used in the x - and y - directions while perfect matching layer (PML) boundaries are used in the propagation z -direction. The mesh step was set to 5 nm. The unit cells were illuminated from the bottom by two pairs of orthogonally polarized plane waves. To achieve full 2π phase coverage, the radii of the cylinders were swept to obtain the corresponding phase and transmission efficiency. Phase responses were extracted through a point monitor at the transverse plane of height $z = 3 \mu\text{m}$. Phase values were computed by extracting the transmission electrical field components and calculating with $\arctan[\text{Im}(E_x)/\text{Re}(E_x)]$. The phase and transmission efficiency were measured sequentially with a 5 nm radius step, then we can obtain the phase changes of unit cells from the fitted phase curve. As shown in Fig. 2(a), all the four cases maintain the same phase control over the complete $0 \sim 2\pi$ range with the cylinder radius varying from 40 nm to 108 nm. The simulated curve of relationship between phase and radius is close to the theoretical curve. As shown in Fig. 2(b), all the four cases maintain the same transmission efficiency, which is over 80% mostly. Therefore, the cylinder unit cell can assure a polarization-independent response.

In order to verify the polarization-insensitivity of the whole metasurface, we used the same incident sources above to generate OVs. A metasurface with size of $20 \mu\text{m} \times 20 \mu\text{m}$ was applied in the simulation. The PML boundary conditions were applied along all three axes. The mesh step was set to 40 nm. A Gaussian beam with a waist radius of $5 \mu\text{m}$ was used as the incident source, the corresponding far-field electrical field distribution was obtained through a field monitor at $10 \mu\text{m}$ away from the metasurface. As shown in Fig. 3, the intensity and phase distributions

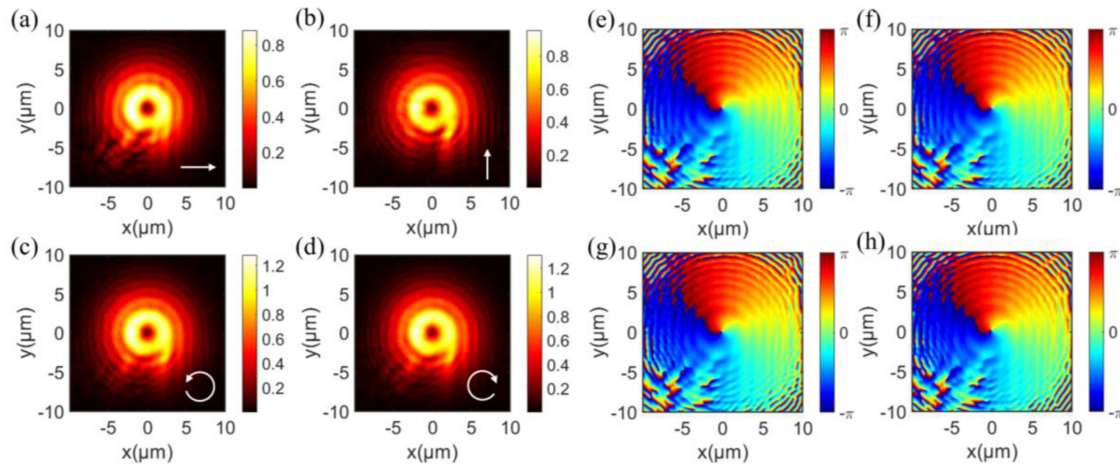


Fig. 3. The (a), (b), (c), (d) intensity and (e), (f), (g), (h) E_x phase distributions in the x - y plane ($z = 10 \mu\text{m}$) of the generated OVs ($l = 1$), with the incidence of x -polarized, y -polarized, left-handed circularly polarized and right-handed circularly polarized beams, respectively.

of the generated OVs are consistent, providing direct evidence that the generated OVs are not affected by the incident polarization states. Although the rotational symmetry is not existing for the whole metasurface, the symmetry break of the metasurface does not have a significant impact on the polarization-independent performance of our metasurface. Based on the above investigations, we can safely confirm the polarization insensitivity of the metasurface. Based on the polarization-insensitive metasurfaces, we generated normal OVs, vector OVs, focused OVs and Bessel OVs, which will be described in the following sections.

3.2 Generation of Normal OVs

Firstly, we generated OVs with the incidence of a Gaussian beam with a waist radius of $5 \mu\text{m}$. The spiral phase profiles of metasurfaces were designed with topological charges 2 and 5 (prime numbers) according to Eq. (1), as shown in the right-bottom inserts of Fig. 4(b) and (e). Clear doughnuts can be seen in Fig. 4(a) and (d), the radii of the maximum intensity rings are about $2.8 \mu\text{m}$ and $3.7 \mu\text{m}$, respectively, as the larger the topological charge the larger the size of the OV ring. The nonuniform efficiency of the metasurfaces prevent the formation of perfect doughnut shape. There are 2 and 5 dark spots inside the rings of the generated OVs with topological charges 2 and 5, respectively. These may be caused by the destructive interferences due to the discontinuous spiral phase. As shown in Fig. 4(b) and (e), the obtained phase distributions are basically consistent with the designed phase distributions. The phases experience 2 and 5 periods of 2π in the circular directions, respectively, indicating the topological charges of the generated OVs are 2 and 5, respectively, which agree with the designed topological charges. As shown in Fig. 4(c) and (f), the measured polarization distributions of the transmitted fields maintain mainly along x -direction, indicating the polarization-insensitive metasurface has almost no effect on the polarization. These results demonstrate that OVs of arbitrary topological charges can be generated by the metasurfaces with cylinder arrays.

3.3 Generation of Vector OVs

Secondly, we generated two most typical vector OVs, radially and azimuthally polarized OVs, by using the metasurface with the topological charge $l = 2$ spiral phase profile above. User-defined electric and magnetic field distributions were used as incident sources. As shown in Fig. 5(a) and

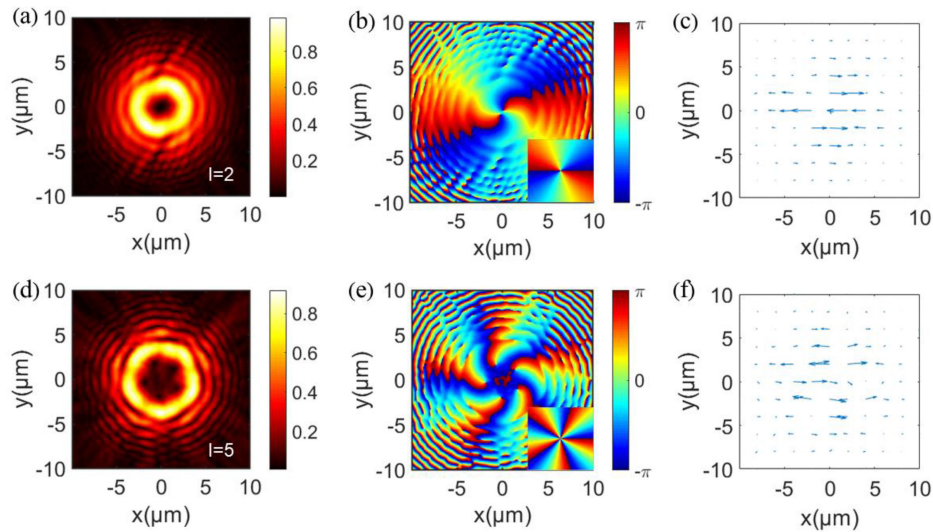


Fig. 4. The (a)(d) intensity, (b), (e) E_x phase distributions in the x - y plane ($z = 10 \mu\text{m}$), and (c), (f) polarization distribution in the x - y plane ($z = 1 \mu\text{m}$) of the generated OVs with topological charges $l = 2$ and $l = 5$, respectively. The inserts at the right-bottom corners of (b), (e) represent the phase distributions of the designed metasurfaces.

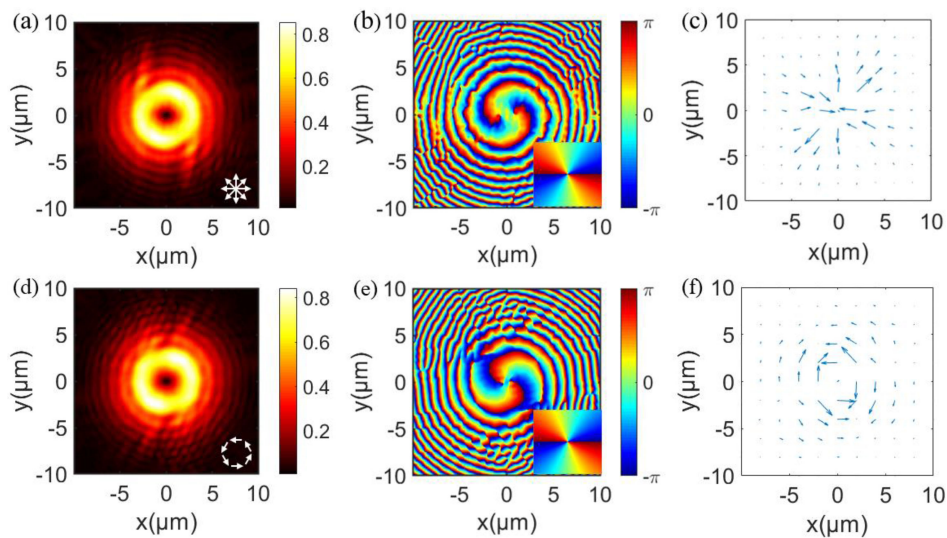


Fig. 5. The (a), (d) intensity, (b), (e) E_z phase distributions in the x - y plane ($z = 10 \mu\text{m}$), and (c), (f) polarization distribution in the x - y plane ($z = 1 \mu\text{m}$) of the generated OVs ($l = 2$) with the incidence of radially and azimuthally polarized beams, respectively. The inserts at the right-bottom corners of (b), (e) represent the phase distributions of the designed metasurfaces.

(d), the incidence of cylindrical vector beams will not prevent the formation of doughnut beams. Compared to previous method using Pancharatnam-Berry (PB) phase metasurface, our method does not rely on the incident polarization. As shown in Fig. 5(b) and (e), the phases experience 2 periods of 2π in the circular directions, indicating the topological charge of the generated OVs is 2, which agrees with the designed topological charge. The generated OVs have similar intensity and phase distributions, confirming the polarization insensitivity of the metasurface. As shown in

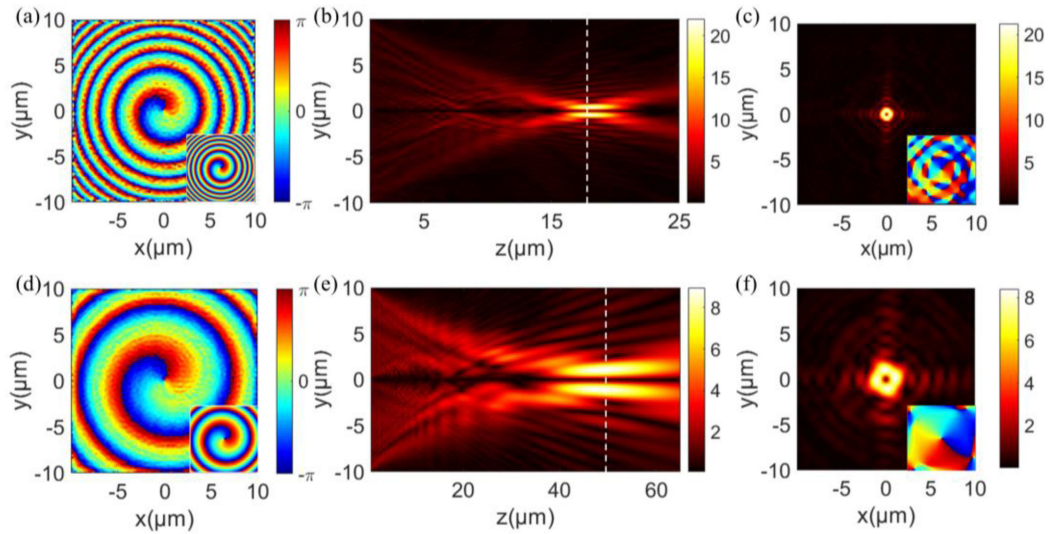


Fig. 6. Simulation results of focused OVs ($l = 1$) with different focal lengths by the incident plane waves. (a), (d) The phase distributions in the x - y planes at $z = 1 \mu\text{m}$, (b), (e) the intensity distributions in the propagating y - z planes, and (c), (f) the intensity distributions in the focal x - y planes, for focal lengths $f = 20 \mu\text{m}$ and $f = 60 \mu\text{m}$, respectively. The inserts at the right-bottom corners of (a), (d) represent the corresponding designed phase profiles. The white dotted lines in (b), (e) denote the focal planes. The inserts at the right-bottom corners of (c), (f) indicate the corresponding phase distributions at the central $5 \mu\text{m} \times 5 \mu\text{m}$ area.

Fig. 5(c) and (f), the measured polarization distributions of the transmitted fields maintain mainly along radial and azimuthal directions, respectively. The slight changes of polarization distributions indicate slight polarization effect for vector beams. Therefore, the phase changes for vector beams and the intensity distributions of vector OVs have slight differences. However, they are still distinguished from normal OVs shown in Fig. 4. This is a direct wavefront control of vector beams by polarization-insensitive metasurfaces, which adds new possibility to the application of structured light.

3.4 Generation of Focused OVs

Thirdly, we generated focused OVs with different focal lengths. In order to verify the function of phase modulation through the second half of Eq. (4), the metasurfaces were designed with the same topological charge $l = 1$ but different focal lengths $20 \mu\text{m}$ and $60 \mu\text{m}$. A plane wave was used as the incident source in the simulation. Fig. 6(a) and (d) show the measured phase distribution above the metasurfaces, which are consistent with the designed phase profiles shown in the right-bottom inserts. Fig. 5(b) and (e) show the electrical fields in the propagation direction, and the focal points are located at about $z = 18 \mu\text{m}$ and $z = 50 \mu\text{m}$, respectively, which are slightly different than the designed focal lengths. Fig. 6(c) and (f) show tiny OVs at the focal plane with the same topological charge $l = 1$, which can be estimated in the enlarged phase distributions. It can be concluded that the focal length and topological charge of the focused OV can be independently controlled, which lays the basis for three-dimensional optical tweezers application.

3.5 Generation of Bessel OVs

Lastly, we generated Bessel OVs with different non-diffraction distances. In order to verify the function of phase modulation through the second half of Eq. (5), the metasurfaces were designed with the same topological charge 1 but different base angles 10° and 15° . A plane wave was used

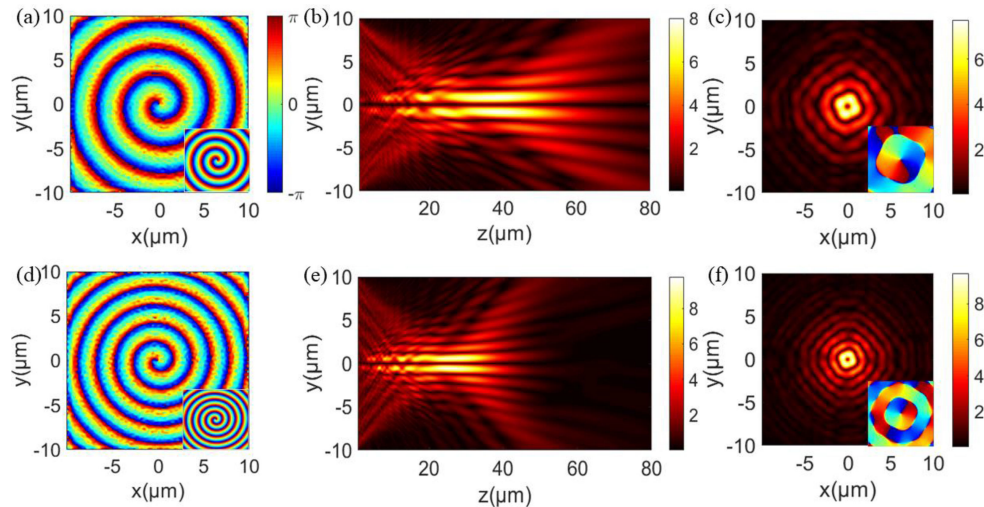


Fig. 7. Simulation results of Bessel OVs ($l = 1$) with different base angles by the incident plane waves. (a), (d) The phase distributions in the x - y planes at $z = 10 \mu\text{m}$, (b), (e) the intensity distributions in the propagating y - z planes, and (c), (f) the intensity distributions in the x - y planes at $z = 10 \mu\text{m}$, for base angles $\beta = 10^\circ$ and $\beta = 15^\circ$, respectively. The inserts at the right-bottom corners of (a), (d) indicate the corresponding designed phase profiles. The inserts at the right-bottom corners of (c), (f) indicate the corresponding phase distributions at the central $5 \mu\text{m} \times 5 \mu\text{m}$ area.

as the incident source in the simulation. Fig. 7(a) and (d) show the measured phase distributions just above the metasurfaces, which are consistent with the designed phase profiles shown in the right-bottom inserts. As can be seen from Fig. 7(b) and (e), the generated Bessel OV is capable of concentrating energy over a distance in the direction of propagation. The enlargement of the beam radius resulting from the diffraction is then overcome, this is of importance for the application in optical communication. The non-diffraction distance is a key indicator of the quality of a non-diffracting beam. The non-diffraction distances are 90λ and 62λ , respectively, which are inversely proportional to the designed base angles, this is consistent with the axicon non-diffraction theory. Damped intensity rings can be clearly seen in Fig. 7(c) and (f), both the enlarged phase distributions indicate the topological charge of the generated Bessel OVs is 1, which are consistent with the design. Therefore, a Bessel OV with non-diffraction characteristics can be generated by the polarization-insensitive metasurface, and its non-diffraction distance and topological charge can be adjusted.

4. Conclusion

In summary, we proposed a method that uses polarization-insensitive metasurfaces to generate OVs. The polarization insensitivity of the cylinder unit array structures has been verified. OVs with different topological charges were generated for demonstrating the feasibility of this method. Our proposed method gets rid of the limitation that the incident light has to be specific polarization in previous methods such as using PB phase metasurfaces. In addition, this method works for any input polarization of the incident light, as a result, it can be used with arbitrary light sources without the need for preconditioning of the polarization state of the input, which typically results in a loss of 50% of the light intensity for an unpolarized light input. Vector OVs can be generated directly with the vector beams input. By means of phase superposition, we generated focused OVs and Bessel OVs, which have potential applications in optical trapping and manipulation, and optical communication. The unique method of imprinting the superposed phase profiles into a single flat surface can dramatically reduce the occupying volume of the system. It can be easily combined into a chip to form composite devices with extended functionalities.

Acknowledgment

The authors wish to thank the anonymous reviewers for their valuable suggestions and Prof. Yefeng Yu for his valuable discussions.

References

- [1] M. W. B. L. Allen, R. J. C. Spreeuw, and J. P. Woerdman, "Orbital angular momentum of light and the transformation of Laguerre-Gaussian laser modes," *Phys. Rev. A*, vol. 45, pp. 8185–8189, 1992.
- [2] M. Vasnetsov and K. Staliunas, *Optical vortices*, Nova Science Pub Incorporated, 1999.
- [3] Q. Zhan, "Properties of circularly polarized vortex beams," *Opt. Lett.*, vol. 31, no. 7, pp. 867–869, 2006.
- [4] P. Gregg, P. Kristensen, and S. Ramachandran, "Conservation of orbital angular momentum in air-core optical fibers," *Optica*, vol. 2, no. 3, pp. 267–270, 2015.
- [5] K. T. Gahagan, and G. A. Swartzlander, "Trapping of low-index microparticles in an optical vortex," *J. Opt. Soc. Amer. B*, vol. 15, no. 2, pp. 524–534, 1998.
- [6] K. T. Gahagan, and G. A. Swartzlander, "Simultaneous trapping of low-index and high-index microparticles observed with an optical-vortex trap," *J. Opt. Soc. Amer. B*, vol. 16, no. 4, pp. 533–537, 1999.
- [7] R. P. C. Coerwinkel, M. W. Beijersbergen, M. Kristensen, and J. P. Woerdman, "Helical-wavefront laser beams produced with a spiral phaseplate," *Opt. Commun.*, vol. 112, pp. 321–327, 1994.
- [8] R. P. Singh, S. Roychowdhury, and V. K. Jaiswal, "Optical vortices produced by forked holographic grating and sign of their topological charge," *Indian J. Phys.*, vol. 80, no. 5, pp. 491–494, 2006.
- [9] A. Jesacher, A. Schwaighofer, S. Furhapter, C. Maurer, S. Bernet, and M. Ritsch-Marte, "Wavefront correction of spatial light modulators using an optical vortex image," *Opt. Express*, vol. 15, no. 9, pp. 5801–5808, 2007.
- [10] Q. Wang, X. W. Sun, and P. Shum, "Generating doughnut-shaped beams with large charge numbers by use of liquid-crystal spiral phase plates," *Appl. Opt.*, vol. 43, no. 11, pp. 2292–2297, 2004.
- [11] N. K. Emami *et al.*, "High-efficiency and low-loss gallium nitride dielectric metasurfaces for nanophotonics at visible wavelengths," *Appl. Phys. Lett.*, vol. 111, no. 22, 2017, Art. no. 221101.
- [12] N. Yu *et al.*, "Light propagation with phase discontinuities: Generalized laws of reflection and refraction," *Science*, vol. 334, no. 6054, pp. 333–337, 2011.
- [13] R. Zhao *et al.*, "Nanoscale polarization manipulation and encryption based on dielectric metasurfaces," *Adv. Opt. Mater.*, vol. 6, no. 19, 2018, Art. no. 1800490.
- [14] B. R. Lu *et al.*, "Reconstructing a plasmonic metasurface for a broadband high-efficiency optical vortex in the visible frequency," *Nanoscale*, vol. 10, no. 26, pp. 12378–12385, 2018.
- [15] K. Zhang *et al.*, "Phase-engineered metalenses to generate converging and non-diffractive vortex beam carrying orbital angular momentum in microwave region," *Opt. Express*, vol. 26, no. 2, pp. 1351–1360, 2018.
- [16] X. Zhang, D. Kong, S. Li, and L. Wang, "Generation of vortex beams with multi topological charges, high purity and operating on broadband using a simple silver metasurface," *Optik*, vol. 175, pp. 319–327, 2018.
- [17] Y. Ma, G. Rui, B. Gu, and Y. Cui, "Trapping and manipulation of nanoparticles using multifocal optical vortex metalens," *Sci. Rep.*, vol. 7, no. 1, 2017, Art. no. 14611.
- [18] H. Zhao, B. Quan, X. Wang, C. Gu, J. Li, and Y. Zhang, "Demonstration of orbital angular momentum multiplexing and demultiplexing based on a metasurface in the terahertz band," *ACS Photon.*, vol. 5, no. 5, pp. 1726–1732, 2017.
- [19] D. Zhang, X. Cao, H. Yang, J. Gao, and X. Zhu, "Multiple OAM vortex beams generation using 1-bit metasurface," *Opt. Express*, vol. 26, no. 19, pp. 24804–24815, 2018.
- [20] Y. Zhang, X. Yang, and J. Gao, "Twisting phase and intensity of light with plasmonic metasurfaces," *Sci. Rep.*, vol. 8, no. 1, 2018, Art. no. 4884.
- [21] P. S. Tan, X. C. Yuan, J. Lin, Q. Wang, and R. E. Burge, "Analysis of surface plasmon interference pattern formed by optical vortex beams," *Opt. Express*, vol. 16, no. 22, pp. 18451–18456, 2008.
- [22] P. S. Tan, G. H. Yuan, Q. Wang, N. Zhang, D. H. Zhang, and X. C. Yuan, "Phase singularity of surface plasmon polaritons generated by optical vortices," *Opt. Lett.*, vol. 36, no. 16, pp. 3287–3289, 2011.
- [23] Y. Zhao, J. S. Edgar, G. D. Jeffries, D. McGloin, and D. T. Chiu, "Spin-to-orbital angular momentum conversion in a strongly focused optical beam," *Phys. Rev. Lett.*, vol. 99, no. 7, 2007, Art. no. 073901.
- [24] Z. Shen, Z. J. Hu, G. H. Yuan, C. J. Min, H. Fang, and X. C. Yuan, "Visualizing orbital angular momentum of plasmonic vortices," *Opt. Lett.*, vol. 37, no. 22, pp. 4627–4629, 2012.
- [25] Y. Zhang *et al.*, "A plasmonic spanner for metal particle manipulation," *Sci. Rep.*, vol. 5, 2015, Art. no. 15446.
- [26] Y. Jiang, X. Li, and M. Gu, "Generation of sub-diffraction-limited pure longitudinal magnetization by the inverse Faraday effect by tightly focusing an azimuthally polarized vortex beam," *Opt. Lett.*, vol. 38, no. 16, pp. 2957–2960, 2013.
- [27] K. E. Chong *et al.*, "Polarization-independent Silicon metadevices for efficient optical wavefront control," *Nano Lett.*, vol. 15, no. 8, pp. 5369–5374, 2015.
- [28] K. E. Chong *et al.*, "Efficient polarization-insensitive complex wavefront control using Huygens' metasurfaces based on dielectric resonant meta-atoms," *ACS Photon.*, vol. 3, no. 4, pp. 514–519, 2016.
- [29] X. Yin, L. Chen, and X. Li, "Polarization-controlled generation of airy plasmons," *Opt. Express*, vol. 26, no. 18, pp. 23251–23264, 2018.
- [30] Y. F. Yu, A. Y. Zhu, R. Paniagua-Dominguez, Y. H. Fu, B. Luk'yanchuk, and A. I. Kuznetsov, "High-transmission dielectric metasurface with 2π phase control at visible wavelengths," *Laser Photon. Rev.*, vol. 9, no. 4, pp. 412–418, 2015.
- [31] Y. Liang *et al.*, "High-efficiency, near-diffraction limited, dielectric metasurface lenses based on crystalline Titanium Dioxide at visible wavelengths," *Nanomaterials*, vol. 8, no. 5, 2018, Art. no. 288.

- [32] E. Arbabi, A. Arbabi, S. M. Kamali, Y. Horie, and A. Faraon, "Multiwavelength polarization-insensitive lenses based on dielectric metasurfaces with meta-molecules," *Optica*, vol. 3, no. 6, pp. 628–633, 2016.
- [33] O. Ahmet, Y. Nazmi, K. Hasan, and K. Hamza, "Polarization-insensitive beam splitters using all-dielectric phase gradient metasurfaces at visible wavelengths," *Opt. Lett.*, vol. 43, no. 18, pp. 4350–4353, 2018.
- [34] I. Tanriover and H. V. Demir, "Broad-band polarization-insensitive all-dielectric metalens enabled by intentional off-resonance waveguiding at mid-wave infrared," *Appl. Phys. Lett.*, vol. 114, no. 4, 2019, Art. no. 043105.
- [35] H. F. Zhang *et al.*, "Polarization-independent all-silicon dielectric metasurfaces in the terahertz regime," *Photon. Res.*, vol. 6, no. 1, pp. 24–29, 2018.
- [36] Z. B. Fan *et al.*, "Silicon Nitride metalenses for close-to-one numerical aperture and wide-angle visible imaging," *Phys. Rev. Appl.*, vol. 10, no. 1, 2018, Art. no. 014005.
- [37] E. B. Grann, M. G. Moharam, and D. A. Pommet, "Optimal design for antireflective tapered two-dimensional subwavelength grating structures," *J. Opt. Soc. Amer. A*, vol. 12, no. 2, pp. 333–339, 1995.
- [38] J. R. Marcianite and D. H. Raguin, "High-efficiency, high-dispersion diffraction gratings based on total internal reflection," *Opt. Lett.*, vol. 29, no. 6, pp. 542–544, 2004.
- [39] J. Plaats, *Fundamentals of optical fiber communications*, Academic Press, 1981.
- [40] Z. Jaroszewicz and J. Morales, "Lens axicons: systems composed of a diverging aberrated lens and a perfect converging lens," *J. Opt. Soc. Amer. A*, vol. 15, no. 9, pp. 2383–2390, 1998.
- [41] M. V. Berry, M. R. Jeffrey, and L. G. Lunney, "Conical diffraction: Observation and theory," *Proc. R. Soc. A*, vol. 462, pp. 1629–1642, 2006.
- [42] K. Zhang *et al.*, "Phase-engineered metalenses to generate converging and non-diffractive vortex beam carrying orbital angular momentum in microwave region," *Opt. Express*, vol. 26, no. 2, pp. 1351–1360, 2018.